W-shaped solitons generated from a weak modulation in the Sasa-Satsuma equation

Li-Chen Zhao,[1] Sheng-Chang Li,[2] and Liming Ling[3,*]
[1]*Department of Physics, Northwest University, 710069, Xi'an, China*
[2]*School of Science, Xi'an Jiaotong University, 710049, Xi'an, China*
[3]*School of Mathematics, South China University of Technology, 510640, Guangzhou, China*
(Received 17 November 2015; revised manuscript received 25 January 2016; published 14 March 2016)

We study rational solutions of continuous wave backgrounds with the critical frequencies of the Sasa-Satsuma equation, which can be used to describe the evolution of the optical field in a nonlinear fiber with some high-order effects. We find a striking dynamical process that two W-shaped solitons are generated from a weak modulation signal on the continuous wave backgrounds. This provides a possible way to obtain stable high-intensity pulses from a low-intensity continuous wave background. The process involves both modulational instability and modulational stability regimes, in contrast to the rogue waves and W-shaped solitons reported before which involve modulational instability and stability, respectively. Furthermore, we present a phase diagram on a modulational instability spectrum plane for the fundamental nonlinear localized waves obtained already in the Sasa-Satsuma equation. The interactions between different types of nonlinear localized waves are discussed based on the phase diagram.

DOI: 10.1103/PhysRevE.93.032215

I. INTRODUCTION

Recently, rational solutions of the nonlinear Schrödinger equation (NLSE) have been paid much attention, since they can be used to describe rogue wave (RW) dynamics in many different physical systems [1–7]. Among these different systems, optical fiber plays an important role in experimental observations for its well-developed intensity and phase modulation techniques. The experimental studies in nonlinear fiber showed that the simplified NLSE could describe the dynamics of localized waves well, which contains only the group velocity dispersion (GVD) and self-phase modulation (SPM). But for ultrashort pulses whose durations are shorter than 100 fs, which is tempting and desirable to improve the capacity of high-bit-rate transmission systems, the nonlinear susceptibility will produce higher-order nonlinear effects like the Kerr dispersion (i.e., self-steepening) and the delayed nonlinear response except for SPM, and even the third-order dispersion (TOD). These are the most general terms that have to be taken into account when extending the applicability of the NLSE [8,9]. With these effects, the corresponding integrable equation was derived as the Sasa-Satsuma (S-S) equation [10].

The linearized stability analysis for the S-S equation in Ref. [11] suggested that there were both modulational instability (MI) and modulational stability (MS) regimes for low perturbation frequencies on the continuous wave background (CWB). In the MI regime, rational solutions were obtained in [12] and [13], which corresponded to RW excitation. It was demonstrated that the high-order effects could make the RW twisted, and the rational solution of the S-S equation had distinctive properties in contrast to those of the well-known NLSE. In the MS regime, we presented rational solutions which corresponded to W-shaped soliton (WS) excitation [14]. It was shown that the profile of the WS depended on the background frequency. The results suggested that not all rational solutions of the nonlinear partial equation corresponded to RW dynamics. Furthermore, it should be noted that there are two critical background frequencies on the boundary of MI and MS regimes for resonant perturbations (see Fig. 3 for details). We expect that there are some new dynamics on CWBs with these critical frequencies.

In this paper, we study the rational solution of the S-S model on CWBs with the critical frequencies. We report a striking dynamical process where two WSs are generated from a weak modulation signal on the CWBs. The striking process involves both MI and MS regimes, in contrast to the RWs and WS reported before which involve MI and MS, respectively. The dynamics process is proven numerically to be robust against white noise. Furthermore, we present a phase diagram on the MI spectrum plane for the fundamental nonlinear excitations obtained already in the S-S equation, mainly including RW with two peaks, Akhmediev breather (AB), Kuznetsov-Ma breather (K-M), WS, W-shaped soliton train (WST), antidark soliton (AD), and stable periodic waves. Based on the phase diagram, we discuss the interactions between different types of nonlinear localized waves through deriving an exact nonlinear superposition solution.

Our presentation of the above features will be structured as follows. In Sec. II, we describe the theoretical model and present the dynamical process for which two WSs are generated from a weak modulation. The underlying mechanism is discussed and the corresponding spectrum evolution is also presented. Furthermore, we test the robustness of the process numerically. In Sec. III, we present a phase diagram on the MI spectrum plane for the fundamental nonlinear excitations already obtained in the S-S equation. The interactions between different types of nonlinear localized waves are investigated based on an exact nonlinear superposition solution. Finally, we summarize the results and present our conclusions in Sec. IV.

II. TWO W-SHAPED SOLITONS GENERATED FROM A WEAK MODULATION ON CWB

For ultrashort pulses whose durations are shorter than 100 fs, the optical field [i.e., $E(t,z)$] in a nonlinear fiber

*Corresponding author: linglm@scut.edu.cn

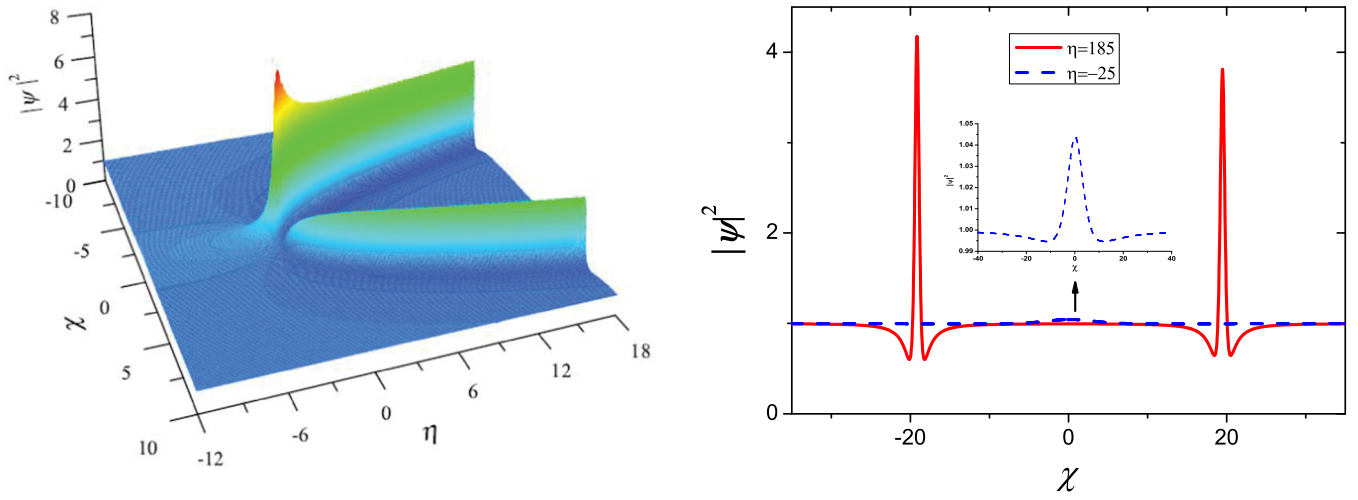

(a) (b)

FIG. 1. (a) The evolution of $|\psi|^2$ [given by Eq. (3)] corresponding to the process that one weak modulation signal evolves into two W-shaped solitons. (b) Cut plots of the localized wave at $\eta = -25$ and $\eta = 185$. It is seen that two W-shaped solitons are generated from a weak modulation. The parameters are $a = \gamma_1 = \gamma_2 = 1$.

with some certain high-order effects can be described by the following S-S model [8–10,15]:

$$iE_z + \tfrac{1}{2}E_{tt} + |E|^2E + i\epsilon[E_{ttt} + 3(|E|^2E)_t + 3|E|^2E_t] = 0, \quad (1)$$

where ϵ is an arbitrary real parameter to scale the integrable perturbations of the NLSE and it can be used to change the strength of the high-order effects conveniently. The last three high-order terms correspond to the TOD, self-steepening, and delayed nonlinear response, respectively [8,15–17]. The Raman effect $T_R E|E|_t^2$ (T_R is a real constant) is not considered in the model, since the term can be much smaller than the Kerr dispersion effect, and it makes the pulse energy nonconservation (this usually makes the model nonintegrable). When $\epsilon = 0$, the S-S equation reduces to the standard NLSE, which has only the terms describing the second-order dispersion and self-phase modulation. It should be clear that the S-S equation is not a general equation that describes nonlinear propagation in optical fibers when high-order terms are present. The relation among these high-order effects should be very specific in order for the equation governing the propagation to become the S-S model, and therefore the optical fiber where the S-S model applies is very special. But studies on the S-S model can still present us some important implications regarding nonlinear localized waves in fiber with these high-order effects [12,13,18,19]. The investigations of the S-S equation indicated that the nonlinear waves in nonlinear fiber with the high-order effects are much more diverse than those in the simplified NLSE [15,17,20–22]. Here, we revisit a rational solution of the S-S model.

For convenience, to observe the following dynamical process, let $\psi(\chi,\eta) = E(t,z)\exp[-\frac{i}{6\epsilon}(t - \frac{z}{18\epsilon})]$ [23], where $\eta = -\frac{3}{2}a^3\epsilon z$ and $\chi = a[t - (\frac{1}{12\epsilon} + \frac{33}{4}a^2\epsilon)z]$. Then Eq. (1) can be rewritten as a complex derivative modified Korteweg–de Vries equation:

$$\psi_\eta = -\frac{11}{2}\psi_\chi + \frac{2}{3}\psi_{\chi\chi\chi} + \frac{2}{a^2}(|\psi|^2\psi)_\chi + \frac{2}{a^2}|\psi|^2\psi_\chi. \quad (2)$$

The coordinates transformation only lead to a trivial phase multiplication between the solutions of Eqs. (2) and (1), and the identical dynamics are kept well. Subsequently, we discuss the nonlinear dynamics of Eq. (2) instead of Eq. (1) without losing generality. Since Galilean transformation is broken for the S-S equation, it is essential to investigate the dynamics of a localized wave on a CWB $\psi_0(\chi,\eta) = a\exp[i\omega_0\chi - i(\frac{3}{2}\omega_0 + \frac{2}{3}\omega_0^3)\eta]$ with arbitrary ω_0. RWs with two peaks [12,13] and rational W-shaped solitons [14] were reported on the CWB with different background frequency regimes. Surprisingly, in the case of $\omega_0 = \pm\frac{1}{2}$ (the critical background field frequencies will be shown below), we find a dynamical process that one weak modulation signal on the CWB can evolve into two stable nonlinear waves as shown in Fig. 1. This dynamical process is very different from the dynamics of nonlinear waves for the same model reported in Refs. [12–14]. From Fig. 1, we see that the propagating signal at the locations before $\eta = -2$ stays weak while it evolves to a large localized wave near $\eta = -1.5$. In particular, this large localized wave splits into two quasistabilized nonlinear waves after $\eta = -1.5$. It is found that the higher peak of the two waves decreases with increasing the propagation distance η while the lower peak increases. However, after a certain distance, their changing rates will tend to zero, namely, the nonlinear localized waves tend to solitons whose shapes are kept well. Their profiles can be observed clearly with the help of making cut plots at a certain location η [see Fig. 1(b)]. The weak modulation form at $\eta = -25$ is shown by the blue dashed line in Fig. 1(b). We emphasize that there is only one modulation signal for the two generated solitons. The profile for soliton shows a nice W-shaped configuration, which is similar to those reported in Ref. [14]. As an example, we show the profile at

$\eta = 185$ by a red solid line in Fig. 1(b). This process suggests one way to excite quasistabilized WSs is through adding a weak modulation on the CWB, which has significant and potential values in the field of soliton applications.

The above dynamical process can be described by the following analytical solution on the CWBs with frequencies $\omega_0 = \pm\frac{1}{2}$, which can be obtained by adopting the Darboux transformation method:

$$\psi(\chi,\eta) = a\left[1 + \frac{H}{M}\right]\exp\left[i\left(\pm\frac{\chi}{2} \mp \frac{5}{6}\eta\right)\right], \qquad (3)$$

with

$$\begin{aligned} H =\ & H_1(\chi,\sqrt{3}\eta) + (2i\sqrt{3} - 12i\chi - 12i\gamma_2 - 6)\gamma_1 \\ & + [18i\chi^2 - (18i\sqrt{3} + 18)\chi - 12\sqrt{3}i\eta + 6\sqrt{3} + 6i]\gamma_2 \\ & + (12i\chi - 8i\sqrt{3} - 12)\gamma_2^2, \\ M =\ & M_1(\chi,\sqrt{3}\eta) + 12\gamma_1^2 + (12\chi^2 - 16\sqrt{3}\chi + 20)\gamma_2^2 \\ & + [(16\sqrt{3} - 24\chi)\gamma_2 + 24\sqrt{3}\eta - 12\chi^2 \\ & + 16\sqrt{3}\chi - 8]\gamma_1 + [12\chi^3 - 24\sqrt{3}\chi^2 \\ & + (48 - 24\sqrt{3}\eta)\chi + 48\eta - 8\sqrt{3}]\gamma_2, \end{aligned}$$

where

$$\begin{aligned} H_1(\chi,\eta) =\ & 6i\chi^3 - (9i\sqrt{3} + 9)\chi^2 + (6\sqrt{3} + 6i - 12i\eta)\chi \\ & + (2i\sqrt{3} - 6)\eta + 2i\sqrt{3} - 6, \\ M_1(\chi,\eta) =\ & 3\chi^4 - 8\sqrt{3}\chi^3 + (24 - 12\eta)\chi^2 \\ & + (16\sqrt{3}\eta - 8\sqrt{3})\chi + 4 - 8\eta + 12\eta^2, \end{aligned}$$

where γ_1 and γ_2 are two real constants. This solution is distinctive from the solutions presented previously in [8,12–14,15,17]. The RW solutions and W-shaped solitons obtained before cannot be reduced to the solution here, since the background frequency must be in some certain regimes for the RW or WS solutions [12–14]. The CWB background frequencies are distinctive from the previous results, and the dynamical process is also distinctive from the previously reported processes. The reasons are discussed in the following paragraph for understanding the dynamical process. When $a = \gamma_1 = \gamma_2 = 1$, the dynamics of solution (3) corresponds to that in Fig. 1. For $a \neq 1$ and other values of $\gamma_{1,2}$, this solution demonstrates the identical dynamical process except for some trivial shifts on the temporal-spatial plane. Performing asymptotic analysis on the exact solution, we find that the two WSs have identical profiles with $\eta \to \infty$. Their hump intensities and valley intensities tend to be 4 and $\frac{5}{8}$ times the CWB intensity value, respectively. This analysis indicates that the two W-shaped localized waves indeed evolve into solitons.

As shown in Ref. [14], the spectrum of WS corresponded to one stable broad spectrum pulse. This means that the two WSs correspond to two broad spectrum pulses, which can be proved by making a Fourier transformation on two asymptotic soliton forms of the exact solution. Since there are two WSs generated from a weak modulation signal, one expects two stable triangular spectrum and interference fringes to emerge. The spectrum evolution of the dynamical process can be obtained exactly through the Fourier transformation $F(\omega,\eta) = \frac{1}{\sqrt{2\pi}}\int_{-\infty}^{+\infty}\psi(\chi,\eta)\exp[-i\omega\chi]dt$. The background's transformation part is integrated to be $\delta(\omega - \omega_0)$ (here the background frequency $\omega_0 = \frac{1}{2}$), and therefore we can eliminate the δ function by taking the transformation on the varying part. We show the evolution of spectrum $\sqrt{|F(\omega,\eta)|}$ in Fig. 2. It is seen that the expected interference pattern on the spectral distribution indeed exists. Specifically, there is a sharp discontinuity for the spectrum and the spectrum is also asymmetric. This is similar to those of RW with double peaks presented in [14,19].

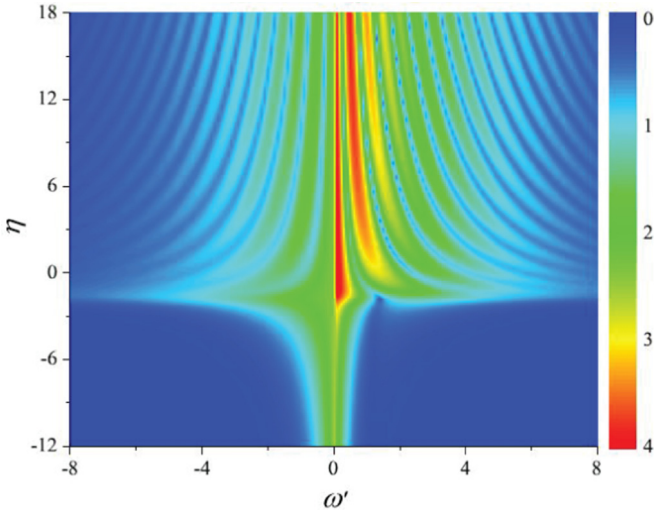

FIG. 2. The corresponding spectrum evolution $\sqrt{|F(\omega,\eta)|}$ of the process illustrated in Fig. 1. It is seen that there is an interference pattern on the spectral distribution. The parameter $\omega' = \omega - \omega_0$.

Now we try to understand the above process for which two WSs are excited from a weak perturbation. We perform the linear stability analysis (LSA) on the CWB $\psi_0(\chi,\eta)$ by adding the Fourier modes with small amplitudes [11], i.e., $f_+\exp[i\omega'(\chi - K\eta)] + f_-^*\exp[-i\omega'(\chi - K^*\eta)]$. The MI gain spectrum $\mathrm{Im}[K]$ is shown on background frequency ω_0 and perturbation frequency ω' space [Fig. 3(a)]. There are two distinctive regimes for perturbations on the continuous background, namely, the MI and MS regimes. The critical points for background frequency are $\omega_0 = \pm\frac{1}{2}$, as shown in Fig. 3(b). For $|\omega_0| \leqslant \frac{1}{2}$, it exists as a MS regime for which the perturbations with arbitrary frequencies are all stable on the CWB. In this regime, stable rational W-shaped soliton solutions were obtained in Ref. [14]. For $|\omega_0| > \frac{1}{2}$, there is a MI regime in which the perturbations with frequencies belonging to $[\omega_0 - \sqrt{4 - \omega_0^{-2}}, \omega_0 + \sqrt{4 - \omega_0^{-2}}]$ are all unstable. The maximum gain of MI in the form $\mathrm{Im}[K]$ emerges on the "resonant" line for which the perturbation frequency is equal to the CWB's. The resonant line in the MI regime usually corresponds to RW excitation. In this regime, RW solutions which possess double humps were given in Refs. [13] and [12]. Notably, the above process for which two WSs grows from a weak perturbation is quite different from the RW and WS dynamics [12–14]. We can qualitatively know that the first stage of the process is in the MI regime, for which the weak modulation signal grows to a strong localized wave with one high hump and two deep valleys, and then it splits. The second stage of the process should evolve in the MS regime, which makes the split localized waves tend to be stable and evolve

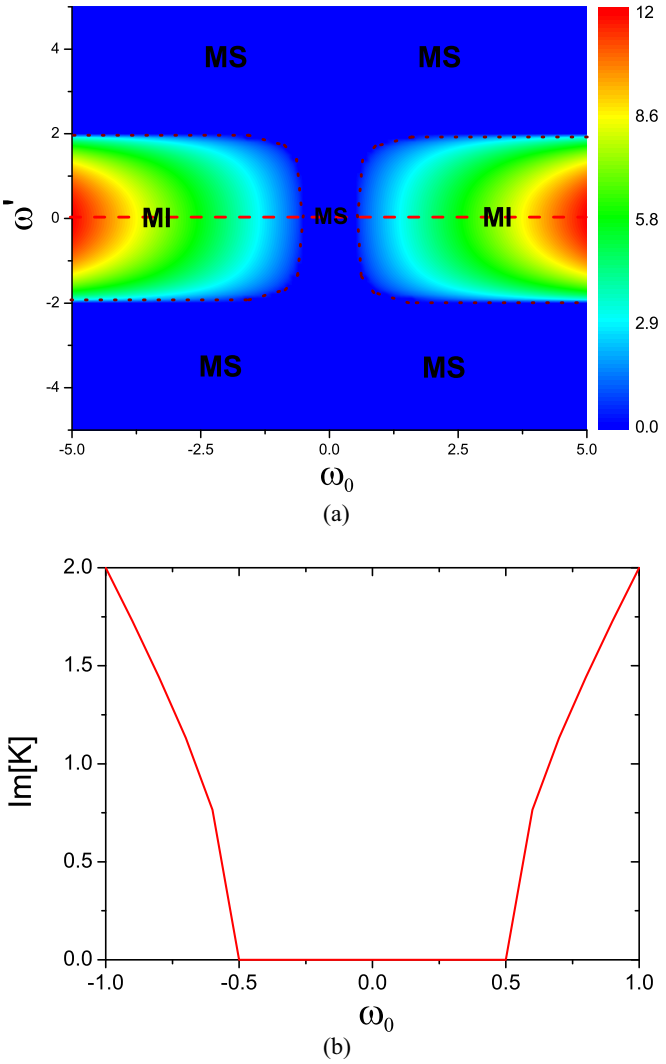

FIG. 3. (a) The MI gain Im[K] distribution on background frequency ω_0 and perturbation frequency ω' plane. The crossing points of the purple dotted lines and the red dashed line are the critical points between MI and MS for resonant perturbation frequency. (b) The cut plot of MI gain on $\omega' = 0$. It is clearly shown that the critical points are at $\pm 1/2$.

into two WSs. The dynamical process is found on the CWB with the critical frequencies $\omega_0 = \pm\frac{1}{2}$, which are located on the boundary between the MS and MI regimes. This indicates that MI and MS can coexist on the critical background frequencies given by the linear stability analysis. The MI analysis of Eq. (1) shows that the MS regime for low-frequency perturbations does not exist when neglecting the high-order effects, mainly including the TOD, self-steepening, and delayed nonlinear response. This implies that these high-order effects play important roles in the dynamical process.

To see the feasibility of process for WSs generation, we numerically evolve Eq. (2) from an exact initial signal at certain locations for which the signals are weak by adopting the split-step Fourier method. To demonstrate the growing process and splitting process clearly, we show the numerical results for $|\psi|^2$ from $\eta = -3$ to $\eta = 3$ in Fig. 4(a), compared with the analytical solution [see Fig. 4(b)]. Figure 5 demonstrates

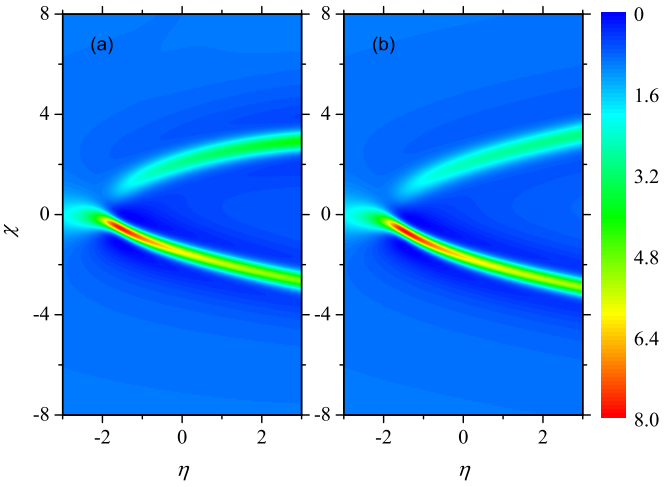

FIG. 4. (a) The numerical simulation for the dynamics of $|\psi(\chi,\eta)|^2$ evolved from an initial data given by the exact solution at $\eta = -3$. (b) The corresponding evolution given by the exact analytical result. It is shown that they agree well with each other, which indicates that the exact signal evolution can survive even with numerical deviations.

the profile comparisons at different locations between the numerical results and the exact results. It is shown that the simulation results agree well with the analytical results, even with numerical deviations. Furthermore, we test the stability of the generated W-shaped solitons with adding white noise 0.01 $Random(\chi)$ ($\chi \in [-1,1]$). As an example, we show the deviations between the numerical result with and without the noise in Fig. 6. The numerical evolutions are from the initial conditions that $\psi_1(\chi,-3) = \psi(\chi,-3)$ and $\psi_2(\chi,-3) = \psi(\chi,-3)(1 + 0.01\, Random[\chi])$, respectively. We can see that the derivations are less than 0.04 in Fig. 6, which agrees with the order of noises. Therefore, the process is stable against noise. This suggests that the exact process might be realized in experiments.

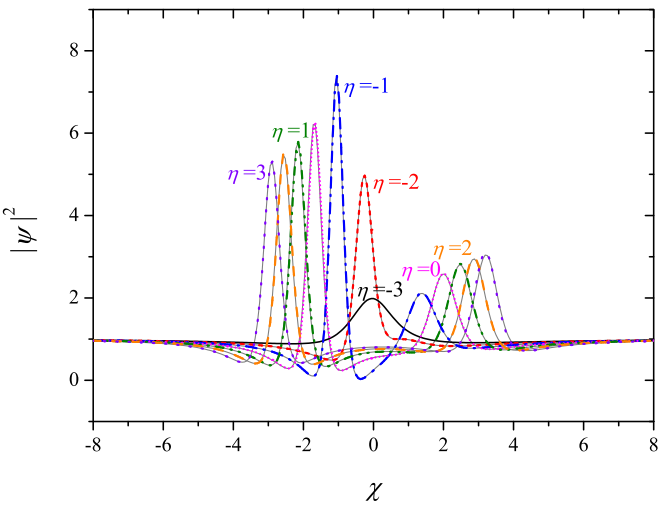

FIG. 5. The profiles of the nonlinear waves at different distances. The solid curves denote the analytical solutions while the dashed or dotted curves correspond to the numerical results. It is seen that the numerical results agree well with the exact analytical results.

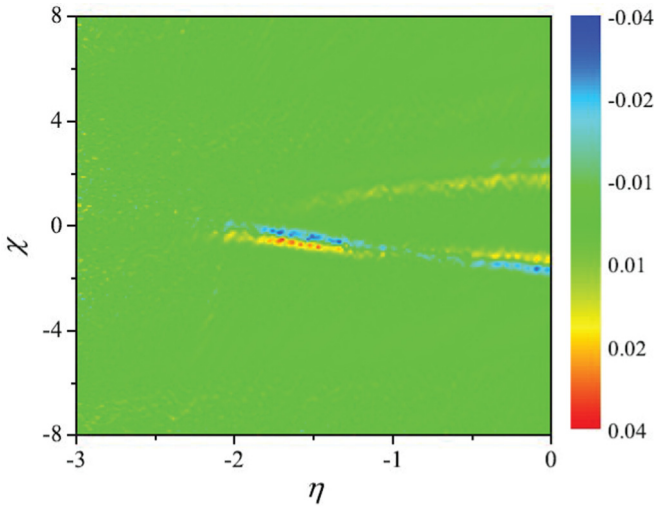

FIG. 6. The deviations between $|\psi_1|^2$ and $|\psi_2|^2$. The numerical evolutions are from the initial conditions that $\psi_1(\chi,-3) = \psi(\chi,-3)$ and $\psi_2(\chi,-3) = \psi(\chi,-3)(1 + 0.01\ Random[\chi])$. It is shown that the deviations are lower than 0.04.

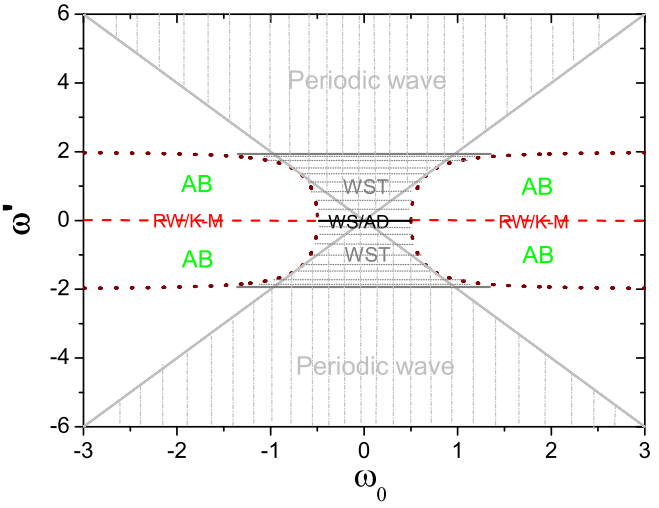

FIG. 7. The phase diagram for nonlinear waves on modulational instability gain spectrum plane. AB, RW, and K-M denote Akhmediev breather, Peregrine rogue wave, and Kuznetsov-Ma breather respectively. WS, WST, AD, and periodic wave denote W-shaped soliton, W-shaped soliton train, antidark soliton, and stable periodic waves, respectively. These nonlinear waves of the S-S equation are all placed clearly on the MI plane. It should be noted that RW and K-M cannot be distinctive from each other on the plane, but their differences can be clarified by dominant propagation constants of them. WS and AD can be distinctive from each other by the temporal or spectral profile. The boundary lines are all obtained explicitly (see related paragraph).

III. A PHASE DIAGRAM ON MODULATIONAL INSTABILITY SPECTRUM FOR LOCALIZED WAVES IN SASA-SATSUMA EQUATION

Until now, many different fundamental localized waves have been found on CWBs in the S-S equation, mainly including RW with two peaks [12,13], AB, K-M, WS [14], WST, AD, and stable periodic waves [24]. Moreover, high-order nonlinear excitations have also been studied in [25]. The dynamics of these localized waves demonstrated that the high-order effects indeed bring some new dynamics in the nonlinear fibers. Recently, we gave an interesting diagram on the MI gain plane for types of fundamental localized waves for the standard NLSE [26] through defining and calculating the dominant frequency and propagation constant of each localized wave. In a similar way, based on Fourier analysis of the exact solutions of RW, AB, K-M, WS, WST, AD, and periodic waves, we can locate these different fundamental nonlinear excitations on the MI plane [Fig. 3(a)], shown in Fig. 7. It should be pointed out that the system admits a stable continuous wave phase in all MS regimes shown in Fig. 3(a). We do not show it in Fig. 7, since there are some nontrivial nonlinear excitations in the MS regimes.

We can see that the RW still comes from the resonance perturbation in MI regimes [26]. AB and K-M dynamics are similar to those of NLSE. We locate RW and K-M on the red dashed line, and the AB is still in the regime between the red dashed line and the purple dotted lines. These are similar to the RW, AB, and K-M for the NLSE case [26]. But there is a MS band with a finite width between the two MI regimes for the S-S model, which brings some new nonlinear excitations for the model. The boundary lines for MI and MS can be calculated as $\omega' = \pm\frac{\sqrt{4\omega_0^2-1}}{\omega_0}$ (see the purple dotted lines). We proved that WS existed on the black solid line in Fig. 7 [14]. Moreover, AD can be also located on the resonant line. The WST is located in the MS regime marked by horizontal short-dotted lines, which are located at the regimes between the resonant line and the boundary line between the MI and MS regimes. The periodic wave is located in the MS regime marked by vertical short-dashed lines. The two boundary lines for the periodic wave can be given as $\omega' = \pm 2\omega_0$ (see the inclined gray solid lines). There is a crossing regime for the WST and periodic wave (see Fig. 7). We can see that WS, AD, WST, and the periodic wave are all located at the MS regime, and their dynamics indeed do not show any evolution instability. Additionally, the periodic wave can admit very high modulation frequencies in the MS regime. This has never been obtained in a standard NLS systems [26]. The above results for two WSs growing from a weak modulation are found on the critical crossing points of the black solid line and the red dashed line in Fig. 7.

From Fig. 7, it is naturally expected that nonlinear interactions of different types of localized waves can be investigated, since there are many different fundamental excitation patterns on a continuous wave background with a certain frequency ω_0. For $\omega_0 \in [-0.5,0.5]$, we can investigate the interactions between any two of WS, AD, WST, and a periodic wave. For $|\omega_0| > 0.5$, one can investigate interactions between any two of RW, AB, K-M, and a periodic wave. But it is not possible to observe the interaction between WS and RW or AB, since WS is not admitted on the background with the frequency $|\omega_0| > 0.5$. Therefore, the corresponding relations between MI and these fundamental nonlinear excitations in Fig. 7 can be used to make a judgment on which types of nonlinear localized waves can coexist and interact with each other. The nonlinear superposition of them can be obtained exactly through the Darboux transformation method [27,28]. We present an exact solution in the Appendix, which can

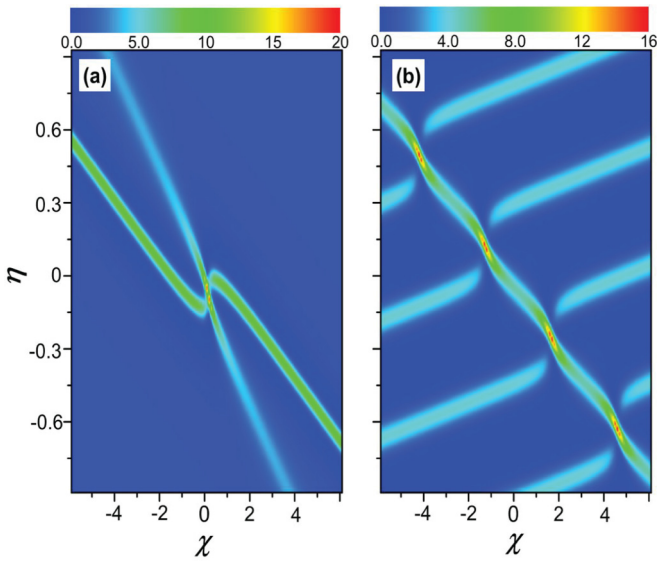

FIG. 8. (a) The interaction between a W-shaped soliton and antidark soliton. Parameters $\omega_0 = \frac{1}{4}$, $k_1 = \frac{1}{13}(5 + 12i)$, $l_1 = \frac{1}{5}(3 + 4i)$, $d_1 = e_1 = 0$, $e_3 = d_3 = -d_2 = -e_2 = 1$. (b) The interaction between a W-shaped soliton and a periodic wave. Parameters $\omega_0 = \frac{1}{4}$, $k_1 = \frac{1}{13}(12 + 5\mathrm{i})$, $l_1 = \frac{1}{5}(3 + 4i)$, $d_1 = e_1 = 0$, $e_3 = d_3 = d_2 = -e_2 = 1$.

describe nonlinear superposition of these nonlinear waves. Based on the solution, we can observe the interaction of different types of localized waves through choosing different parameters. For example, we show two cases in Fig. 8 which correspond to the interaction between WS and AD [Fig. 8(a)] or a periodic wave [Fig. 8(b)]. These results have not been found in NLSE described systems. The interaction between them can be inelastic or elastic [24,25]. Their explicit interaction properties are out of the scope of this paper. We will discuss these interaction properties in the future.

Additionally, K-M can admit strong perturbation on a CWB. The linear MI analysis fails to predict the stability of perturbations with different propagation constants, especially for strong perturbations. This is because the analysis just provides implications on the stability of weak perturbations with different frequencies. New tools still need to be developed to analyze the stability of perturbations with different propagation constants [29]. For example, it was shown that WS or AD could coexist and interplay with a breather [24]. The breather is in the MS regime on the above MI gain plane. It seems that there is a contradiction with the MI analysis. However, the mechanism for this type of breather is distinctive from those for AB and RW, and this type breather cannot be reduced to RW anyway. We suggest that the breathing behavior along the evolution direction comes from the interference effect between CWB and the perturbation and is induced by their propagation constant difference. This is supported by the analysis of the dominant propagation constant of the breather solution. Moreover, the MI analysis can be used just to understand the amplifying process of weak perturbations for nonlinear localized waves, but it cannot explain their whole dynamical process. It is still needed to develop some new ways to understand the whole dynamical process of fundamental RW and even high-order processes [30,31].

IV. CONCLUSION AND DISCUSSION

In summary, we present a striking dynamical process for which two WSs are generated from a weak modulation signal on CWBs with critical frequencies $\omega_0 = \pm\frac{1}{2}$. The numerical simulations indicate that the dynamical process is robust against weak noises or perturbations. The underlying mechanisms of the process are discussed qualitatively based on MI analysis. The process involves MI to MS autonomously. This indicates that MI and MS can coexist on the critical background frequency given by LSA. The striking dynamical process suggests that there could also be some new dynamics on the critical frequencies between the MI and MS regimes for other nonlinear systems [32–34]. Notably, the critical frequencies located on the boundary between the MS and MI regimes are obtained by LSA. The analysis predicts that there is no MI on the critical frequencies, but we demonstrate that both MI and MS play key roles in the dynamical process. This means that LSA does not stand precisely on the boundary lines between the MI and MS regimes. The explicit underlying mechanism for the dynamical process still needs new analysis techniques.

Actually, many recent experiments for nonlinear localized waves, including K-M, AB, and Peregrine RW in nonlinear fibers [3,35,36], have provided a good platform to investigate the complicated dynamics of nonlinear localized waves on a CWB. Those experimental works suggest that the exact analytical solutions for the simplified NLSE could describe the evolution of optical fields well even with nonideal initial conditions. The ideal initial conditions are important to study the NLSE with high-order effects, and the present work provides the initial conditions for generating WSs from certain weak modulations in experiments. This has been checked numerically even for the initial conditions with little noise. In particular, our theoretical results can be used to qualitatively understand a recent experiment in a nonlinear fiber with TOD and self-steepening effects [37]. In the experiment, one Peregrine RW split into two lower-amplitude localized solitons and the pulse splitting process was explained by high-order MI based on a high-order AB solution of the simplified NLSE [38]. Here, we provide another perspective for understanding the pulse splitting process and predicting the quasistability of the splitting pulses with certain high-order effects.

Finally, we present a phase diagram on the MI spectrum plane for the fundamental nonlinear localized waves obtained in the S-S equation, which is in sharp contrast to that for standard NLSE [26]. This is because these high-order effects cause the MI plane for S-S to be quite different from that for NLSE. (There is a MS band with a finite width between MI regimes for S-S, which is absent for the NLSE.) Furthermore, we discuss interactions between different types of nonlinear waves based on the phase diagram. The results will further enrich our understanding of nonlinear excitation dynamics in S-S model systems.

ACKNOWLEDGMENTS

We are grateful to Dr. Tao Xu for his helpful discussions. This work is supported by the National Science Foundation of China (Contracts No. 11405129, No. 11305120, and No.

11401221) and through Fundamental Research Funds for the Central Universities of China.

APPENDIX

Through performing the Darboux transformation twice [27–29], an exact nonlinear superposition solution of the S-S equation can be presented as

$$\psi[2]=\left[\frac{H_{11}H_{22}-H_{12}H_{21}}{F_{11}F_{22}-F_{12}F_{21}}\right]e^{i\omega_0[\chi-(\frac{2}{3}\omega_0^2+\frac{3}{2})\eta]},$$

where

$$F_{11}=\sum_{i,j=1}^{3,3}\frac{d_id_je^{X_i^*+X_j}}{\mu_j-\mu_i^*},\quad F_{12}=\sum_{i,j=1}^{3,3}\frac{d_ie_je^{X_i^*+Y_j}}{\nu_j-\mu_i^*},$$

$$F_{21}=\sum_{i,j=1}^{3,3}\frac{e_id_je^{Y_i^*+X_j}}{\mu_j-\nu_i^*},\quad F_{22}=\sum_{i,j=1}^{3,3}\frac{e_ie_je^{Y_i^*+Y_j}}{\nu_j-\nu_i^*},$$

and

$$H_{11}=\sum_{i,j=1}^{3,3}\frac{d_id_j(\mu_i^*+\omega_0)e^{X_i^*+X_j}}{(\mu_j-\mu_i^*)(\mu_j+\omega_0)},$$

$$H_{12}=\sum_{i,j=1}^{3,3}\frac{d_ie_j(\mu_i^*+\omega_0)e^{X_i^*+Y_j}}{(\nu_j-\mu_i^*)(\nu_j+\omega_0)},$$

$$H_{21}=\sum_{i,j=1}^{3,3}\frac{e_id_j(\nu_i^*+\omega_0)e^{Y_i^*+X_j}}{(\mu_j-\nu_i^*)(\mu_j+\omega_0)},$$

$$H_{22}=\sum_{i,j=1}^{3,3}\frac{e_ie_j(\nu_i^*+\omega_0)e^{Y_i^*+Y_j}}{(\nu_j-\nu_i^*)(\nu_j+\omega_0)}.$$

$d_i,e_i\in\mathbb{R}$. The expressions of X_i are

$$X_i=i\mu_i\left[\chi-\left(\tfrac{2}{3}(\omega_0^2+2\lambda_1\mu_i)+\tfrac{17}{6}\right)\eta\right],$$

where $\lambda_1=\frac{\omega_0(k_1-1)}{2(k_1+1)}+\frac{(k_1^2-1)}{4\omega_0k_1}$,$\mu_1=\frac{\omega_0(k_1-1)}{k_1+1}$,$\mu_2=\frac{k_1^2-1+\sqrt{\Delta_1}}{4\omega_0k_1}$, $\mu_3=\frac{k_1^2-1-\sqrt{\Delta_1}}{4\omega_0k_1}$, $\Delta_1=(4\omega_0^2k_1+k_1^2-1)^2+16\omega_0^2k_1(k_1+1)$ ($|k_1|=1,k_1\neq\pm1$).

The expressions of Y_i are

$$Y_i=i\nu_i\left[\chi-\left(\tfrac{2}{3}(\omega_0^2+2\lambda_2\nu_i)+\tfrac{17}{6}\right)\eta\right],$$

where $\lambda_2=\frac{\omega_0(k_2-1)}{2(k_2+1)}+\frac{(k_2^2-1)}{4\omega_0k_2}$, $\nu_1=\frac{\omega_0(k_2-1)}{k_2+1}$, $\nu_2=\frac{k_2^2-1+\sqrt{\Delta_2}}{4\omega_0k_2}$, $\nu_3=\frac{k_2^2-1-\sqrt{\Delta_2}}{4\omega_0k_2}$, $\Delta_2=(4\omega_0^2k_2+k_2^2-1)^2+16\omega_0^2k_2(k_2+1)$ ($|k_2|=1,k_2\neq\pm1$). This solution describes interaction between different types of nonlinear waves which can coexist on the same background field. The correspondence relations between MI and the fundamental nonlinear excitations in Fig. 7 can be used to make a judgment regarding which types of nonlinear localized waves can coexist and interact with each other.

[1] M. Onorato, S. Residori, U. Bortolozzo, A. Montina, and F. T. Arecchi, Phys. Rep. **528**, 47 (2013).

[2] D. R. Solli, C. Ropers, P. Koonath, and B. Jalali, Nature (London) **450**, 1054 (2007).

[3] B. Kibler, J. Fatome, C. Finot *et al.*, Nat. Phys. **6**, 790 (2010).

[4] H. Bailung, S. K. Sharma, and Y. Nakamura, Phys. Rev. Lett. **107**, 255005 (2011).

[5] A. Chabchoub and N. Akhmediev, Phys. Lett. A **377**, 2590 (2013).

[6] A. Chabchoub, N. Hoffmann, M. Onorato, A. Slunyaev, A. Sergeeva, E. Pelinovsky, and N. Akhmediev, Phys. Rev. E **86**, 056601 (2012).

[7] A. Chabchoub, N. Hoffmann, M. Onorato, and N. Akhmediev, Phys. Rev. X **2**, 011015 (2012).

[8] Y. Kodama and A. Hasegawa, IEEE J. Quantum Electron. **23**, 510 (1987).

[9] Y. Kodama, J. Stat. Phys. **39**, 597 (1985).

[10] N. Sasa and J. Satsuma, J. Phys. Soc. Jpn. **60**, 409 (1991).

[11] O. C. Wright, III, Chaos, Solitons Fractals **33**, 374 (2007).

[12] U. Bandelow and N. Akhmediev, Phys. Rev. E **86**, 026606 (2012).

[13] S. H. Chen, Phys. Rev. E **88**, 023202 (2013).

[14] L. C. Zhao, S. C. Li, and L. M. Ling, Phys. Rev. E **89**, 023210 (2014).

[15] K. Porsezian and K. Nakkeeran, Phys. Rev. Lett. **76**, 3955 (1996).

[16] G. P. Agrawal, *Nonlinear Fiber Optics* (Academic Press, New York, 2007).

[17] Z. H. Li, Lu Li, H. P. Tian, and G. S. Zhou, Phys. Rev. Lett. **84**, 4096 (2000).

[18] J. M. Soto-Crespo, N. Devine, N. P. Hoffmann, and N. Akhmediev, Phys. Rev. E **90**, 032902 (2014).

[19] N. Akhmediev, J. M. Soto-Crespo, N. Devine, and N. P. Hoffmann, Phys. D **294**, 37 (2015).

[20] D. Mihalache, L. Torner, F. Moldoveanu, N.-C. Panoiu, and N. Truta, J. Phys. A: Math. Gen. **26**, L757 (1993).

[21] D. Mihalache, N.-C. Panoiu, F. Moldoveanu, and D.-M. Baboiu, J. Phys. A: Math. Gen. **27**, 6177 (1994).

[22] D. Mihalache, L. Torner, F. Moldoveanu, N.-C. Panoiu, and N. Truta, Phys. Rev. E **48**, 4699 (1993).

[23] K. Nakkeeran, K. Porsezian, P. S. Sundaram, and A. Mahalingam, Phys. Rev. Lett. **80**, 1425 (1998).

[24] L. Ling (unpublished).

[25] T. Xu, D. Wang, M. Li, and H. Liang, Phys. Scr. **89**, 075207 (2014); T. Xu, M. Li, and L. Li, Europhys. Lett. **109**, 30006 (2015).

[26] L. C. Zhao and L. M. Ling, arXiv:1410.7536.

[27] V. B. Matveev and M. A. Salle, *Darboux Transformations and Solitons* (Springer, Berlin, 1991).

[28] B. L. Guo, L. M. Ling, and Q. P. Liu, Phys. Rev. E **85**, 026607 (2012); Stud. Appl. Math. **130**, 317 (2013).

[29] V. E. Zakharov and A. A. Gelash, Phys. Rev. Lett. **111**, 054101 (2013).

[30] G. Biondini and D. Mantzavinos, Phys. Rev. Lett. **116**, 043902 (2016).

[31] B. Kibler, A. Chabchoub, A. Gelash, N. Akhmediev, and V. E. Zakharov, Phys. Rev. X **5**, 041026 (2015).

[32] L. C. Zhao, Z. Y. Yang, and L. M. Ling, J. Phys. Soc. Jpn. **83**, 104401 (2014).
[33] C. Liu, Z. Y. Yang, L. C. Zhao, and W. L. Yang, Phys. Rev. E **91**, 022904 (2015).
[34] C. Liu, Z. Y. Yang, L. C. Zhao, and W. L. Yang, Ann. Phys. (NY) **362**, 130 (2015).
[35] B. Kibler, J. Fatome, C. Finot, G. Millot, G. Genty, B. Wetzel, N. Akhmediev, F. Dias, and J. M. Dudley, Sci. Rep. **2**, 463 (2012).
[36] J. M. Dudley, G. Genty, F. Dias, B. Kibler, and N. Akhmediev, Opt. Express **17**, 21497 (2009).
[37] K. Hammani, B. Kibler, C. Finot, P. Morin, J. Fatome, J. M. Dudley, and G. Millot, Opt. Lett. **36**, 112 (2011).
[38] M. Erkintalo, K. Hammani, B. Kibler, C. Finot, N. Akhmediev, J. M. Dudley, and G. Genty, Phys. Rev. Lett. **107**, 253901 (2011).